Carbohydrate Polymers 80 (2010) 270–275

Contents lists available at ScienceDirect

Carbohydrate Polymers

journal homepage: www.elsevier.com/locate/carbpol

Synthesis of cellulose–calcium silicate nanocomposites in ethanol/water mixed solvents and their characterization

Shu-Ming Li [a], Ning Jia [a], Jie-Fang Zhu [b], Ming-Guo Ma [a,c,*], Run-Cang Sun [a]

[a] Engineering Research Center of Forestry Biomass Materials and Bioenergy, College of Materials Science and Technology, Beijing Forestry University, Beijing 100083, PR China
[b] Department of Materials Chemistry, The Ångström Laboratory, Uppsala University, Uppsala 75121, Sweden
[c] State Key Laboratory of Pulp and Paper Engineering, South China University of Technology, Guangzhou 510640, PR China

ARTICLE INFO

Article history:
Received 24 September 2009
Received in revised form 24 October 2009
Accepted 17 November 2009
Available online 22 November 2009

Keywords:
Cellulose
Calcium silicate
Nanocomposite

ABSTRACT

Cellulose–calcium silicate nanocomposites with calcium silicate nanoparticles homogeneously dispersed in the cellulose matrix have been successfully synthesized using cellulose solution, $Ca(NO_3)_2{\cdot}4H_2O$ and $Na_2SiO_3{\cdot}9H_2O$ in ethanol/water mixed solvents at room temperature for 24 h. The cellulose solution was previously prepared by the dissolution of cellulose in a solvent system of *N*,*N*-dimethylacetamide (DMAc)/lithium chloride (LiCl). The feeding order had an influence on the morphology of the cellulose–calcium silicate nanocomposites and the size of the calcium silicate particles. The cellulose in nanocomposites showed cellulose type II crystalline structure. The products were characterized by X-ray powder diffraction (XRD), thermogravimetric analysis (TG), differential scanning calorimetric analysis (DSC), Fourier transform infrared spectrometry (FT-IR), energy-dispersive X-ray spectra (EDS), and scanning electron microscopy (SEM).

1. Introduction

As the most abundant renewable material and natural polysaccharide found on earth (Klemm, Heublein, Fink, & Bohn, 2005), cellulose has been receiving considerable attention and becomes one of important materials owing to its unique properties such as chemical stability, mechanical strength, biocompatibility, biodegradation (Gindl & Keckes, 2004; Iguchi, Yamanaka, & Budhiono, 2000; Shoda & Sugano, 2005) and its broad applications in housing, furniture, clothing, solid fuels, fiber, paper, and medical products.

Compared to the individual components, nanocomposites provide the possibility for the enhancement of multifunctional properties due to interaction between the counterparts (Caruso, 2001; Hanif, Meulenberg, & Strouse, 2002; Schmidt et al., 1998) and become a fast-growing field of chemical research due to their interesting optical, electrical, and mechanical properties and many promising potential applications in various fields (Ajayan, Stephan, Redlich, & Colliex, 1995; Sun et al., 2005; Zeng, Li, Liu, Wang, & Sun, 2002).

Recently, the synthesis of cellulose-based nanocomposites has attracted more attention, and many efforts have been placed on the synthesis of the cellulose-based nanocomposites (Daoud, Xin, & Zhang, 2005; Hong et al., 2006; Jiang et al., 2008; Liu, Zhang, Zhou, & Wu, 2008; Marques, Trindade, & Neto, 2006; Tsioptsias & Panayiotou, 2000; Zhang et al., 2007). For example, Liu et al. (2008) reported the synthesis of cellulose/Fe_2O_3 nanocomposite fibers with a higher mechanical strength, superparamagnetic properties, and a relatively high dielectric constant by wet spinning in NaOH/urea aqueous solution. Hong et al. (2006) synthesized hydroxyapatite/bacterial cellulose composites from simulated body fluid (SBF) via a biomimetic route. Zhang et al. (2007) used room temperature ionic liquid AmimCl as solvent for the fabrication of regenerated-cellulose/multiwalled-carbon-nanotube composite fibers with enhanced mechanical properties.

Calcium silicate is used in drug delivery (Jain, Awasthi, Jain, & Agrawal, 2005; Li & Chang, 2005; Ma, Zhu, Li, & Cao, 2008) and bone tissue regeneration (Cortes, Medina, Escobedo, Escobedo, & Lopez, 2004; Kokubo, Kawai, Kawashita, Yamamoto, & Nakamura, 2005; Li et al., 2007; Matsuoka et al., 1999; Oyane et al., 2003) due to its good biocompatibility, bioactivity, and degradability. The cellulose–calcium silicate nanocomposites are considered to have potential applications in biomedical field with such striking features as high mechanical properties and excellent biocompatibility. However, as far as we know, the synthesis of cellulose–calcium silicate nanocomposites has not reported yet.

Herein, we report in detail the synthesis of cellulose–calcium silicate nanocomposites using cellulose solution, $Ca(NO_3)_2{\cdot}4H_2O$ and $Na_2SiO_3{\cdot}9H_2O$ in ethanol/water mixed solvents. The cellulose

* Corresponding author. Address: Engineering Research Center of Forestry Biomass Materials and Bioenergy, College of Materials Science and Technology, Beijing Forestry University, Beijing 100083, PR China. Tel.: +86 10 62336592; fax: +86 10 62338149.
E-mail address: mg_ma@bjfu.edu.cn (M.-G. Ma).

0144-8617/$ - see front matter © 2009 Elsevier Ltd. All rights reserved.
doi:10.1016/j.carbpol.2009.11.024

solution was previously prepared by the dissolution of cellulose in a solvent system of *N*,*N*-dimethylacetamide (DMAc)/lithium chloride (LiCl), since DMAc/LiCl mixed solvents are well known as the solvent system to dissolve cellulose (Terbojevich, Cosani, Conio, Ciferri, & Bianchi, 1985). After that, the cellulose solution was mixed with the ethanol/water mixed solvents. The calcium silicate nanoparticles were synthesized in situ on the surface of the cellulose to obtain the cellulose–calcium silicate nanocomposites.

2. Experimental

2.1. Preparation of cellulose–calcium silicate nanocomposites

All chemicals were of analytical grade and used as received without further purification. All experiments were conducted under air atmosphere. Microcrystalline cellulose (molecular weight of 34,843–38,894, degree of polymerization (*DP*), *DP* = 215–240) of a commercial reagent was purchased from Sinopharm Group Chemical Reagent Co., Ltd., Shanghai, China. A typical synthesis experiment for the cellulose solution was carried out as follows: 1.510 g of LiCl was added into 20 mL of *N*,*N*-dimethylacetamide (DMAc) under vigorous stirring to form LiCl solution. Then, 1.416 g of microcrystalline cellulose was added into the above solution under vigorous stirring. The above solution was heated by an oil bath at 90 °C for 3 h. After cooling to ambient temperature, the obtained regenerated cellulose solution was used for the preparation of cellulose–calcium silicate nanocomposites. The regenerated cellulose was separated from the solution by centrifugation, washed by ethanol several times and dried at 60 °C in vacuum for further characterization.

For the synthesis of cellulose–calcium silicate nanocomposites, the ethanol (60 mL)/distilled water (15 mL) mixed solvents were poured into cellulose solution (5 mL), and then 0.472 g of $Ca(NO_3)_2{\cdot}4H_2O$ and 0.568 g of $Na_2SiO_3{\cdot}9H_2O$ were added into the resulting colloidal solution under vigorous magnetic stirring at room temperature for 24 h. The resulting precipitate was separated from the solution by centrifugation, washed by water and ethanol several times and dried at 60 °C for further characterization.

2.2. Characterization

X-ray powder diffraction (XRD) patterns were recorded in 2θ range from 10° to 70° on a X'Pert PRO MPD diffractometer operating at 40 kV with Cu Kα (λ = 1.5405 Å) radiation. Scanning electron microscopy (SEM) images were recorded with a Hitachi 3400 N scanning electron microscopy. The energy-dispersive X-ray spectra (EDS) attached to the scanning electron microscopy was used to analyze the composition of sample. Fourier transform infrared (FT-IR) spectroscopy was carried out on an FT-IR spectrophotometer (Nicolet 510), using the KBr disk method. Thermal behavior of the cellulose–calcium silicate nanocomposite was performed using thermogravimetric analysis (TGA) and differential scanning calorimetric analysis (DSC) with a STA-409PC/4/H Luxx simultaneous TG-DTA/DSC apparatus (Netzsch, Germany) at a heating rate of 10 °C min^{-1} in flowing air. Thermal behavior of microcrystalline cellulose and regenerated cellulose was performed using thermogravimetric analysis (TGA) and differential thermal analysis (DTA) on a simultaneous thermal analyzer (DTG-60, Shimadzu) at a heating rate of 10 °C min^{-1} in flowing air.

3. Results and discussion

Ethanol is miscible with water at any ratio, and the addition of ethanol to water can easily change the physicochemical properties. The nucleation and growth of the calcium silicate occurred rapidly by the reaction between Ca^{2+} and SiO_3^{2-} in aqueous solution. However, the addition of ethanol to water can restrain the diffusion of Ca^{2+} and SiO_3^{2-} ions, and the nucleation and growth of the calcium silicate. It is well known that rapid nucleation and slow growth favor the formation of particles with small size and narrow size distribution. Moreover, the DMAc is also miscible with water at any ratio. So we choose the ethanol/water mixed solvents as the solvent system.

The average degree of polymerization (*DP*) and molecular weight of the regenerated cellulose were obtained by British standard methods for determination of limiting viscosity number in dilute solution (Part 1. Cupri-ethylenediamine (CED) method) (Evans & Wallis, 1989). The molecular weight of the regenerated cellulose was calculated from their *DP* by multiplying by 162. The value of *DP* of the regenerated cellulose is 118; therefore the molecular weight of the regenerated cellulose is 19,116.

3.1. X-ray powder diffraction characterization

Fig. 1a shows the XRD pattern of the microcrystalline cellulose. The sample indicated three diffraction peaks at around 2θ = 14.9°, 22.5°, and 34.5° as the typical diffraction pattern of cellulose type I. However, the regenerated cellulose had different diffraction pattern from that of the microcrystalline cellulose, as shown in Fig. 1b. The cellulose in Fig. 1b exhibit peaks at 2θ = 20.7° and 22.7°, assigned to the (110) and (200) planes of crystalline cellulose type II (Togawa & Kondo, 1999). Fig. 1c shows the XRD pattern of the cellulose–calcium silicate nanocomposite, which has a similar diffraction pattern of cellulose to Fig. 1b. Moreover, the relatively peak intensity of the cellulose in nanocomposite decreased, compared with Fig. 1b, implying that the incorporated nanoparticles lead to a decrease of the crystallinity of the cellulose due to a strong interaction between nanoparticles and the cellulose matrix. These results indicated that the solvent system of DMAc/LiCl played an important role in the phase transformation of cellulose, in well agreement with the previous reports (Gindl & Keckes, 2005; Terbojevich et al., 1985). The other diffraction peaks of the nanocomposites were assigned to the calcium silicate.

3.2. TGA, DSC, and DTA characterization

The thermal behavior of the cellulose–calcium silicate nanocomposite was investigated with thermogravimetric analysis (TGA) and differential scanning calorimetric analysis (DSC) (Fig. 2). For comparison, the TGA and differential thermal analysis (DTA) curves of microcrystalline cellulose and regenerated cellulose are also shown in Fig. 3. The weight loss at around 120 °C is due to the loss of hydrated and coordinated water molecules, which come from the ambient environment. From TGA curve, it

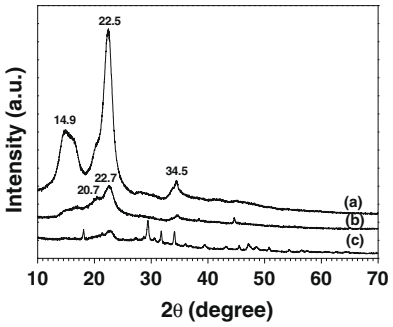

Fig. 1. XRD patterns of (a) the microcrystalline cellulose, (b) the regenerated cellulose, and (c) the cellulose–calcium silicate nanocomposite.

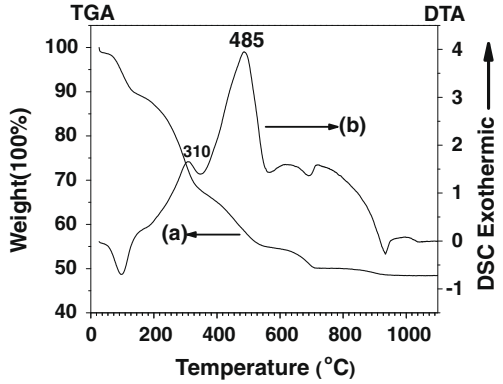

Fig. 2. (a) TGA and (b) DSC curves of the cellulose–calcium silicate nanocomposite.

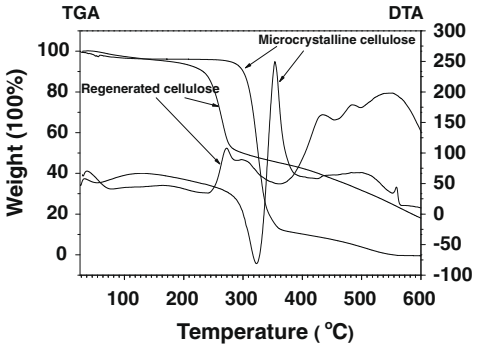

Fig. 3. TGA and DTA curves of the microcrystalline cellulose and the regenerated cellulose.

is also observed that the further weight loss takes place at 310 and 485 °C. The weight loss around 310 °C was probably caused by the thermal degradation of cellulose in the composite. However, the weight loss of microcrystalline cellulose and regenerated cellulose take place in the region 250–380 and 190–310 °C, respectively (Fig. 3). One can see that the degradation temperature in the composite was different from the microcrystalline cellulose and regenerated cellulose, which indicated the formation of the composites with partially disrupting crystalline structure in cellulose. The weight loss around 485 °C can be attributed to the phase transformation of calcium silicate to β-wollastonite. The DSC curve shows broad exothermic peaks located around 310 and 485 °C, respectively. The temperature ranges of the exothermic peaks in the DSC curve fit well with those of weight loss in the TGA curve.

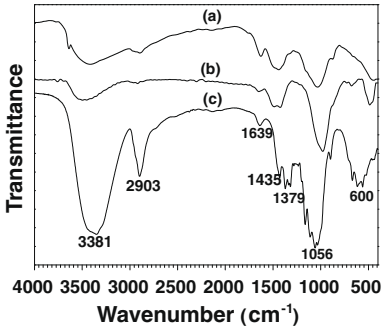

Fig. 4. FT-IR spectra of (a) the cellulose–calcium silicate nanocomposite, (b) calcium silicate, and (c) the microcrystalline cellulose.

3.3. FT-IR characterization

The FT-IR spectra of the cellulose–calcium silicate nanocomposite, calcium silicate and pure microcrystalline cellulose were shown in Fig. 4. The pure microcrystalline cellulose had four strong broad peaks at 3381, 2903, 1056, and 600 cm^{-1} and some weak peaks at 1639, 1435, and 1379 cm^{-1} (Fig. 4c). The strong broad band at 3381 cm^{-1} can be assigned to stretching vibration in OH group of cellulose. The 2903 cm^{-1} belongs to asymmetrically stretching vibration of C–H in pyranoid ring. The broad absorption band around 1056 cm^{-1} is attributed to the C–O of cellulose. The band at 1639 cm^{-1} belongs to the bending mode of adsorbed water. The calcium silicate had six peaks at 3494, 1641, 1499, 1422, 975, and 470 cm^{-1} (Fig. 4b). The band at ~470 cm^{-1} belongs to the bending modes of Si–O–Si and O–Si–O bonds. The band at ~975 cm^{-1} is due to stretching modes of O–Si–O bonds and Si–O–Ca bonds containing non-bridging oxygen, and symmetric stretching vibrations of Si–O–Si bonds. The broad band at 3494 cm^{-1} is attributed to stretching vibration of O–H in calcium silicate.

Fig. 4a shows the FT-IR spectrum of the cellulose–calcium silicate nanocomposite, which exhibits the characteristic absorptions duo to both cellulose and calcium silicate. The band at ~449 cm^{-1} belongs to the bending modes of Si–O–Si and O–Si–O bonds. The characteristic stretching mode of the C–O in cellulose is located at ~1056 cm^{-1}, which is not clearly observed because of the overlapping with the strong band due to the stretching modes of O–Si–O bonds and Si–O–Ca bonds containing non-bridging oxygen, and symmetric stretching vibrations of Si–O–Si bonds. The peak at ~3381 cm^{-1} of cellulose moved to a higher wavenumber and became broader in nanocomposite, compared with Fig. 4c, implying a strong interaction between the OH group of cellulose and calcium silicate nanoparticles through hydrogen bonding.

3.4. Scanning electron microscopy

The SEM micrographs of the cellulose–calcium silicate nanocomposite were shown in Fig. 5. After the ethanol (60 mL)/water (15 mL) mixed solvents were added into the obtained cellulose solution (5 mL), the nanocomposite with rolling morphology was observed (Fig. 5a and b). A magnified micrograph of the nanocomposite was shown in Fig. 5b. One can see that the nanoparticles with diameters about 150 nm were homogeneously dispersed in the cellulose matrix (Fig. 5b).

The EDS spectrum (Fig. 6a) shows that the sample consists of C, Ca, O, and Si, the right composition of cellulose–calcium silicate nanocomposite. Fig. 6b–e show the EDS elemental mapping images of C, Ca, O, and Si, respectively, and further confirm the composition of cellulose–calcium silicate nanocomposite and the even distribution of calcium silicate nanoparticles.

However, when the feeding order was changed, the obtained cellulose solution (5 mL) was added into the ethanol (60 mL)/water (15 mL) mixed solvents, while other reaction conditions were the same, a completely different shape of the nanocomposite was observed (Fig. 7). One can see that the particles with diameters about 2 μm were homogeneously dispersed in the cellulose matrix (Fig. 7a). Fig. 7b shows the detailed structure of Fig. 7a, indicating the particles had polyhedron morphology. These results indicated that the feeding order had an influence on the morphology of the cellulose–calcium silicate nanocomposite and the size of the calcium silicate particles.

The samples in Figs. 5 and 7 were previously treated by ultrasound method, so the SEM results implied that the samples were not mechanical mixtures of cellulose and calcium silicate. It is well known that the cellulose and calcium silicate nanoparticles have

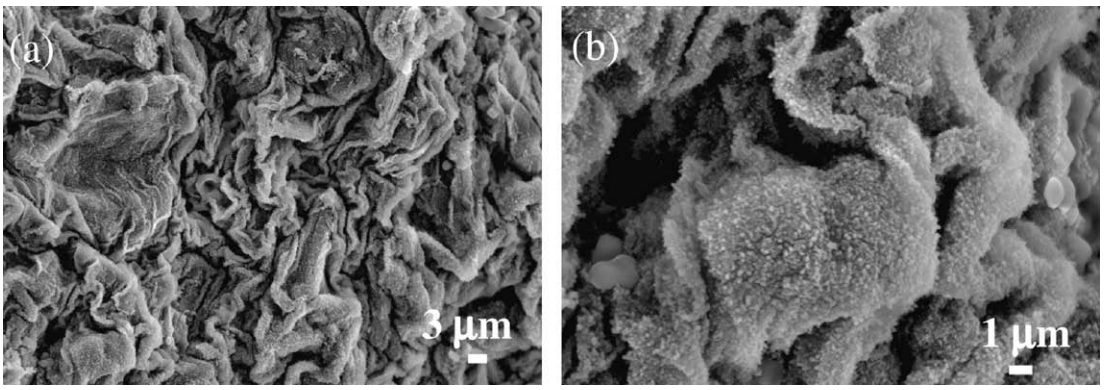

Fig. 5. SEM micrographs of the cellulose–calcium silicate nanocomposite.

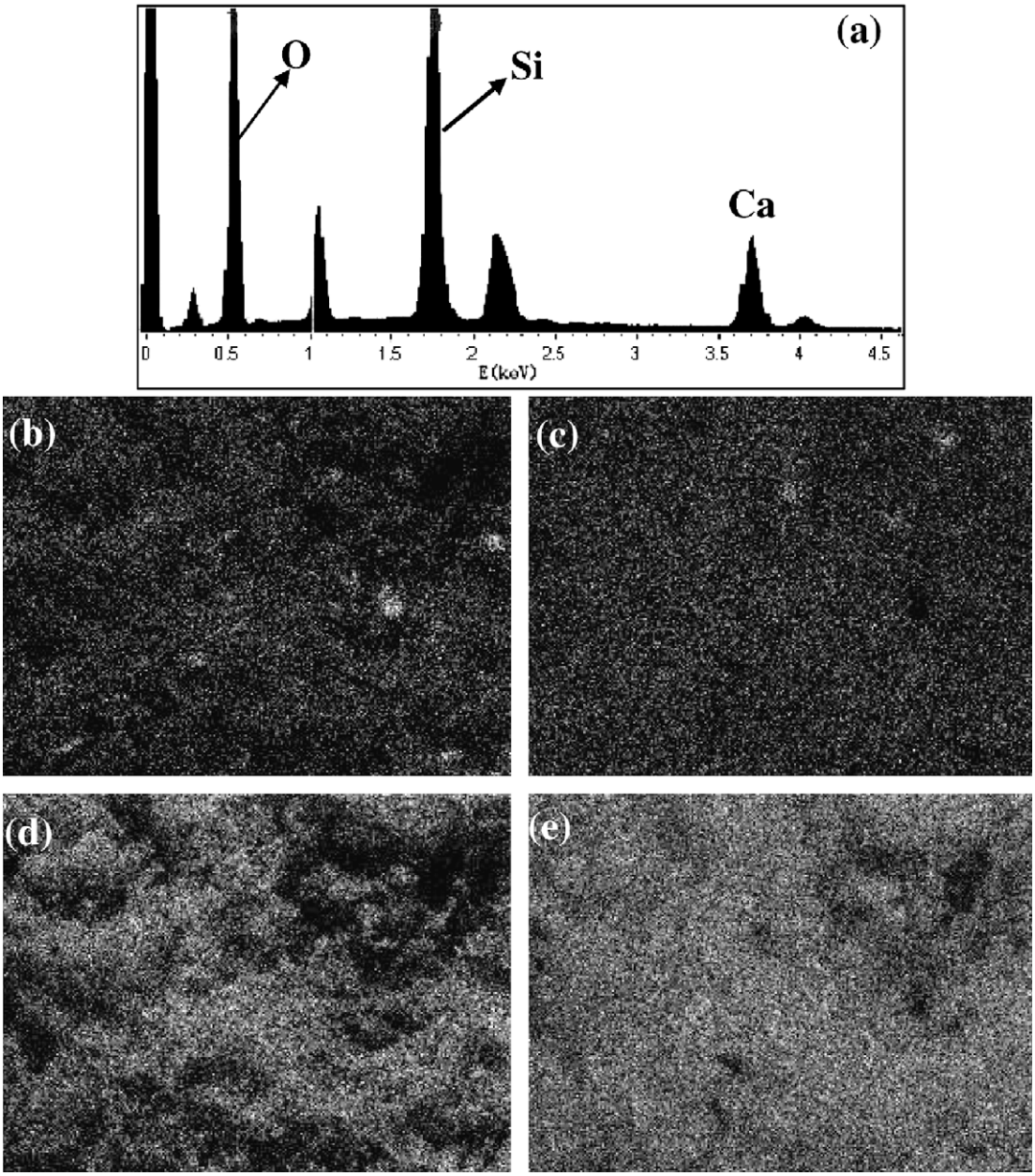

Fig. 6. (a) EDS spectrum and (b–e) the EDS elemental mapping images of the cellulose–calcium silicate nanocomposite: (b) C; (c) Ca; (d) O; and (e) Si.

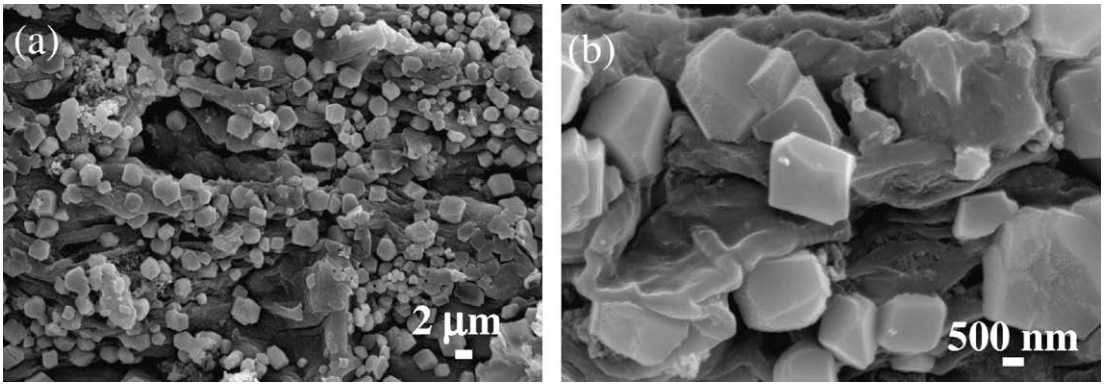

Fig. 7. SEM micrographs of the cellulose–calcium silicate nanocomposite with calcium silicate nanoparticles dispersed in the cellulose matrix prepared by the reversed feeding order, compared with that in Fig. 5.

many surface hydroxyls, which can act as binders, making the cellulose and calcium silicate nanoparticles well conjoint.

4. Conclusions

In summary, we report a simple and reliable route to synthesis of the cellulose–calcium silicate nanocomposites. The nanocomposites were characterized by XRD, TG, DSC, FT-IR, SEM, and EDS analysis. The results indicated that the original crystalline structure of cellulose was disrupted in final nanocomposites prepared. A strong interaction between the OH group of cellulose and calcium silicate nanoparticles through hydrogen bonding were confirmed by FT-IR. The SEM micrographs showed the particles were homogeneously dispersed in the cellulose matrix. The EDS spectrum and EDS elemental mapping images further confirmed the composition of cellulose–calcium silicate nanocomposite. The feeding order had an influence on the morphology and the size of the calcium silicate particles. The cellulose–calcium silicate nanocomposites would be a promising material for biomedical applications.

Acknowledgments

Financial support from the Beijing Forestry University Young Scientist Fund (BLX2W8010), the Special Fund of Basic Scientific Research Operation Expenses of Central Colleges (BLYX200934), China Postdoctoral Science Foundation, Ångpanneföreningen's Foundation for Research and Development (Ref. No. 09-370), Major State Basic Research Development Program of China (973 Program) (No. 2010CB732204), China Ministry of Education (No. 111 project), and the Opening Project of State Key Laboratory of Pulp and Paper Engineering, South China University of Technology (200814) is gratefully acknowledged.

References

Ajayan, P. M., Stephan, O., Redlich, P., & Colliex, C. (1995). Carbon nanotubes as removable templates for metal oxide nanocomposites and nanostructures. *Nature, 375*, 564–567.

Caruso, F. (2001). Nanoengineering of particle surfaces. *Advanced Materials, 13*, 11–22.

Cortes, D. A., Medina, A., Escobedo, J. C., Escobedo, S., & Lopez, M. A. (2004). Effect of wollastonite ceramics and bioactive glass on the formation of a bonelike apatite layer on a cobalt base alloy. *Journal of Biomedical Materials Research A, 70A*, 341–346.

Daoud, W. A., Xin, J. H., & Zhang, Y. H. (2005). Surface functionalization of cellulose fibers with titanium dioxide nanoparticles and their combined bactericidal activities. *Surface Science, 599*, 69–75.

Evans, R., & Wallis, A. F. A. (1989). Cellulose molecular weights determined by viscometry. *Journal of Applied Polymer Science, 37*, 2331–2340.

Gindl, W., & Keckes, J. (2004). Tensile properties of cellulose acetate butyrate composites reinforced with bacterial cellulose. *Composites Science and Technology, 64*, 2407–2413.

Gindl, W., & Keckes, J. (2005). All-cellulose nanocomposite. *Polymer, 46*, 10221–10225.

Hanif, K. M., Meulenberg, R. W., & Strouse, G. F. (2002). Magnetic ordering in doped $Cd_{(1-x)}Co_{(x)}Se$ diluted magnetic quantum dots. *Journal of the American Chemical Society, 124*, 11495–11502.

Hong, L., Wang, Y. L., Jia, S. R., Huang, Y., Gao, C., & Wan, Y. Z. (2006). Hydroxyapatite-bacterial cellulose composites synthesized via a biomimetic route. *Materials Letters, 60*, 1710–1713.

Iguchi, M., Yamanaka, S., & Budhiono, A. (2000). Bacterial cellulose – a masterpiece of nature's arts. *Journal of Materials Science, 35*, 261–270.

Jain, S. K., Awasthi, A. M., Jain, N. K., & Agrawal, G. P. (2005). Calcium silicate based microspheres of repaglinide for gastroretentive floating drug delivery: preparation and in vitro characterization. *Journal of Control Release, 107*, 300–309.

Jiang, L. Y., Li, Y. B., Wang, X. J., Zhang, L., Wen, J. Q., & Gong, M. (2008). Preparation and properties of nano-hydroxyapatite/chitosan/carboxymethyl cellulose composite scaffold. *Carbohydrate Polymers, 74*, 680–684.

Klemm, D., Heublein, B., Fink, H. P., & Bohn, A. (2005). Cellulose: Fascinating biopolymer and sustainable raw material. *Angewandte Chemie International Edition, 44*, 3358–3393.

Kokubo, T., Kawai, M., Kawashita, M., Yamamoto, K., & Nakamura, T. (2005). Fabrics of polymer fibers modified with calcium silicate for bone substitute. *Key Engineering Materials, 284–286*, 775–778.

Li, H. Y., & Chang, J. (2005). Preparation, characterization and in vitro release of gentamicin from PHBV/wollastonite composite microspheres. *Journal of Control Release, 107*, 463–473.

Li, X., Shi, J. L., Zhu, Y. F., Shen, W. H., Li, H., Liang, J., et al. (2007). A template route to the preparation of mesoporous amorphous calcium silicate with high in vitro bone-forming bioactivity. *Journal of Biomedical Materials Research B, 83B*, 431–439.

Liu, S. L., Zhang, L. N., Zhou, J. P., & Wu, R. X. (2008). Structure and properties of cellulose/Fe_2O_3 nanocomposite fibers spun via an effective pathway. *The Journal of Physical Chemistry C, 112*, 4538–4544.

Ma, M. Y., Zhu, Y. J., Li, L., & Cao, S. W. (2008). Nanostructured porous hollow ellipsoidal capsules of hydroxyapatite and calcium silicate: preparation and application in drug delivery. *Journal of Materials Chemistry, 18*, 2722–2727.

Marques, P. A. A., Trindade, T., & Neto, C. P. (2006). Titanium dioxide/cellulose nanocomposites prepared by a controlled hydrolysis method. *Composites Science and Technology, 66*, 1038–1044.

Matsuoka, H., Akiyama, H., Okada, Y., Ito, H., Shigeno, C., Konishi, J., et al. (1999). In vitro analysis of the stimulation of bone formation by highly bioactive apatite- and wollastonite-containing glass-ceramic: released calcium ions promote osteogenic differentiation in osteoblastic ROS17/2.8 cells. *Journal of Biomedical Materials Research, 47*, 176–188.

Oyane, A., Kawashita, M., Nakanishi, K., Kokubo, T., Minoda, M., Miyamoto, T., et al. (2003). Bonelike apatite formation on ethylene-vinyl alcohol copolymer modified with silane coupling agent and calcium silicate solutions. *Biomaterials, 24*, 1729–1735.

Schmidt, H. K., Geiter, E., Menning, M., Krug, H., Becker, C., & Winkler, R. P. (1998). The sol–gel process for nano-technologies: new nanocomposites with interesting optical and mechanical properties. *Journal of Sol–Gel Science and Technology, 13*, 397–404.

Shoda, M., & Sugano, Y. (2005). Recent advances in bacterial cellulose production. *Biotechnology and Bioprocess Engineering, 10*, 1–8.

Sun, Z. Y., Liu, Z. M., Han, B. X., Wang, Y., Du, J. M., Xie, Z. L., et al. (2005). Fabrication of ruthenium–carbon nanotube nanocomposites in supercritical water. *Advanced Materials, 17*, 928–932.

Terbojevich, M., Cosani, A., Conio, G., Ciferri, A., & Bianchi, E. (1985). Mesophase formation and chain rigidity in cellulose and derivatives. 3. Aggregation of

cellulose in *N*,*N*-dimethylacetamide-lithium chloride. *Macromolecules, 18*, 640–646.

Togawa, E., & Kondo, T. (1999). Elastic modulus of the crystalline regions of cellulose polymorphs. *Journal of Polymer Science, Part B: PolymPhys, 33*, 1647–1651.

Tsioptsias, C., & Panayiotou, C. (2000). Preparation of cellulose–nanohydroxyapatite composite scaffolds from ionic liquid solutions. *Carbohydrate Polymers, 74*, 99–105.

Zeng, H., Li, J., Liu, J. P., Wang, Z. L., & Sun, S. H. (2002). Exchange-coupled nanocomposite magnets by nanoparticle self-assembly. *Nature, 420*, 395–398.

Zhang, H., Wang, Z. G., Zhang, Z. N., Wu, J., Zhang, J., & He, J. S. (2007). Regenerated cellulose/multi-walled carbon nanotube (MWCNT) composite fibers with enhanced mechanical properties prepared with an ionic liquid 1-allyl-3-methylimidazolium chloride (AmimCl). *Advanced Materials, 19*, 698–704.